New Physics: Sae Mulli,
Vol. 69, No. 9, September 2019, pp. 957∼963
http://dx.doi.org/10.3938/NPSM.69.957

Finite-Difference Time-Domain Analysis on Grating Coupled Plasmonic System

ByeongChan PARK · Jae-Won JANG*
Department of Physics, Pukyong National University, Busan 48513, Korea

(Received 22 July 2019 : revised 21 August 2019 : accepted 23 August 2019)

In this work, we used a finite-difference time-domain (FDTD) characterization to demonstrate that the e-field near metal nanoparticles (NPs) can be enhanced by dielectric grating structure. An array of Au NPs ($\phi = 60$ nm) with 4 nm gaps is set as a plasmonic system. The Au NP arrays on a flat polydimethylsiloxane (PDMS) substrate and a thin Au film-coated substrate are considered as control samples. Coupling with a PDMS line grating (5 μm × 3 μm × 1 μm = width × gap × height) is carried out by placing the Au NP array on the PDMS grating and by putting the PDMS grating on the Au NP array on a thin Au-film-coated substrate. The dependences of the Wavelength and the angle of incidence of a plane-wave source on the e-field intensity are investigated. For the sample systems in the result, the maximum e-field of the PDMS-grating-coupled samples is enhanced by more than a factor of two compared to that in the control samples. This finding will be helpful to develop e-field-enhancing templates for surface-enhanced raman spectroscopy (SERS) applications.

PACS numbers: 41.20.Jb, 68.65.−k, 78.67.−n, 81.07.−b
Keywords: Finite-difference time-domain simulation, Localized surface plasmon resonance, Grating

I. Introduction

Metal nanoparticles (NPs) have attracted many attentions of scientist and engineers because plasmonic excitation of the metal NPs can be utilized in various applications. Surface-enhanced Raman scattering (SERS) [1–3] is one of the application utilizing the plasmonic excitation of the metal NPs. It is reported that SERS enhancement is available by an electric field (e-field) near the molecule presenting Raman signal. Especially, SERS enhancement is proportional to the power of four of the e-field ($\propto |\mathbf{E}|^4$). [4,5] Hence, localized surface plasmon resonance (LSPR) of metal NPs is used to be utilized for SERS enhancement. [6–8] For example, SERS enhancement becomes stronger by mutual metallic particle interaction such as Au NPs or Ag NPs on a substrate. [6–9] The e-field is significantly amplified between each metallic particle by the interaction called plasmonic coupling, which is based on strengthened electric polarization in the metallic/organic hybrid structure. [10,11] Such an e-field hotspot is a key of SERS enhancement; however, the hotspot is not easy to be obtained and controlled in many SERS structures. One of the solutions to establish the hotspot for SERS enhancement is to use highly ordered metal nanostructures by using advanced nanolithographic techniques [12,13].

In this work, the e-field distribution of plasmonic system comprised of metal NP array is characterized to identify a suitably coupled structure with a grating structure for SERS enhancement by means of finite-difference time-domain (FDTD) analysis. The grating structure is considered to amplify e-field near the plasmonic sample system by interference and diffraction (or in-plane e-field guiding effect [14, 15]). In accordance with favorably empirically achieved fabrication tools and approaches, the array of Au NPs hybrid with a polydimethylsiloxane (PDMS) grating and an Au film-coated substrate, as well as a flat PDMS substrate, are mainly characterized. In the result, it is demonstrated that e-field in the array of

*E-mail: jjang@pknu.ac.kr

metal NPs can be enhanced by coupling with the dielectric grating structure. The enhanced e-field near metal NPs means that SERS enhancement is also available by coupling between plasmonic system (the metal NPs) and the grating structure. Our finding would be useful to design an effective SERS template with utilizing a grating structure.

II. Methods

The e-field distribution of the plasmonic system is measured with two-dimensional (2-D) FDTD simulation using a commercial Maxwell's equation solving software (FDTD Solution, Lumerical Inc., Canada). As the plasmonic sample system, which can be utilized for SERS, arrays of Au NPs (60 nm diameter and 4 nm gap) placed on dielectric PDMS substrate and Au film-coated substrate are used. As the grating structure, PDMS line grating of 5 μm width, 3 μm gap, and 1 μm height is adapted for the FDTD simulations. The two-kinds of samples of grating coupled plasmonic system are designed; one is the array of Au NPs placing on the PDMS grating, and the other is the array of Au NPs on the Au film substrate with the PDMS grating contacting on it. Plane waves with a wavelength of 500 nm, 600 nm, 700 nm, and 800 nm are set as the source and incident angle is varied as 0°, 15°, 30°, 45°, and 60°. To emphasize coupling with the PDMS ling grating, the plane wave source in transverse mode (the e-filed of the source is perpendicular to the line axis of the grating) is only used. The boundary condition of the FDTD simulations is established with perfectly matched layers (PMLs) on top and bottom planes and with Bloch boundary condition on sides. Size of the 2-D FDTD simulation structure is 5 μm length and 8 μm width to the vertical and horizontal directions for the PDMS grating included sample systems. The sample systems without including the PDMS grating, such as the arrays of Au NPs on PDMS substrate and Au film-coated substrate, have the size of 5 μm length and 640 nm width to the vertical and horizontal direction. Refractive index of the PDMS materials is set as 1.41 [16]. Wavelength dependent materials indices of Au, Ti, SiO_2, and Si are determined from the values based on the data reported by Johnson and Christy [17], Weaver and Frederikse (CRC) [18], Palik [19], and Palik [19], respectively. Mesh size used in the all 2-D FDTD simulations is 1 nm^2.

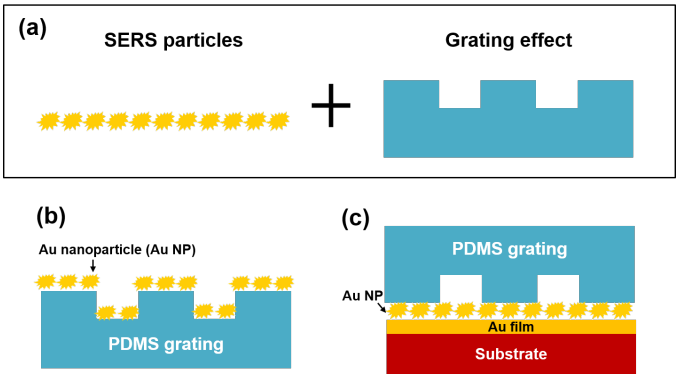

Fig. 1. (Color online) (a) Scheme of the object; grating effect coupled SERS particles (array of metal NPs) to strengthen e-field near the particles for SERS enhancement. (b,c) Examples of the grating effect coupled plasmonic particle systems: (b) Au NPs placing on PDMS grating, (c) PDMS grating contacting on the array of Au NPs placed on Au film-coated substrate.

III. Results and Discussions

Here, it is characterized whether e-field of a plasmonic system, which can be used as a SERS template, can be enhanced by a dielectric grating structure, or not. Figure 1(a) represents the scheme of the object of this study; grating effect influences on SERS particles (array of metal NPs) to strengthen e-field near the particles for SERS enhancement. Model systems of the grating effect coupled SERS particles are displayed in Figs. 1(b) and 1(c). Figure 1(b) shows the array of Au NPs putting on a PDMS grating, where e-field near the Au NPs would be influenced by e-field generated on the surface of the PDMS grating when light irradiates on the grating. In addition, another model system of grating effect coupled SERS particles can be obtained as shown in Fig. 1(c). The array of Au NPs is placed on an Au film-coated substrate, where one can anticipate in e-field enhancement between the Au NPs and the Au film as well as gap of the array of Au NPs by plasmonic excitation if light irradiates on the sample system. To apply for grating effect, a PDMS grating is contacted on the array of the Au NPs, where e-field near the Au NPs would be influenced by e-field generated on the surface of the PDMS grating when light irradiates through the grating.

In order to characterize the e-field enhancement of the grating effect coupled plasmonic systems, FDTD simulations are carried out. As the first step, control experiments are executed. Figure 2 shows the FDTD structures of the sample systems for the control experiments.

One control sample is the array of Au NPs on a PDMS substrate as shown in Fig. 2(a). The PDMS substrate is positioned at 3 μm away from the top PML layer. The dimension of the Au NP array is set-up by 60 nm diameter and 4 nm gap, which is determined with considering empirically obtainable plasmonic particles. In the literature, plasmonic excitation optimized Au NPs are a mostly atypical shape (star, raspberry-like) and their size is 50–80 nm. [20,21] Considering the thickness of surfactant surrounding the plasmonic excitation optimized Au NPs and space between the Au NPs resulted from their atypical shape, 4 nm gap is set-up in the array of Au NPs to imitate the empirically obtainable plasmonic excitation optimized Au NPs. Plane source wave in transverse mode (Fig. 2(a)) inlets above the array of Au NPs on PDMS substrate with controlling wavelength and incident angle. Another control sample is the array of Au NPs on an Au film-coated substrate (Fig. 2(b)). All setting parameters except the Au film-coated substrate are the same as the control sample shown in Fig. 2(a). Total thickness of the Au film-coated substrate is 2 μm as same as that of the PDMS grating. To imitate an actual Au film-coated substrate, 30 nm Au film with 3 nm Ti buffer layer on 300 nm SiO_2 deposited Si substrate (1.667 μm) is set-up for the FDTD simulation. Moreover, as shown in Fig. 2(c), PDMS grating (5 μm width, 3 μm gap, and 1 μm height) is set-up to characterize e-field enhancement near the grating surface depending on wavelength and incident angle of the irradiating light.

As the next step, FDTD simulation with the control sample systems (Fig. 2) is carried out as changing wavelength and incident angle of the source wave. The most enhanced e-field in each wavelength and incident angle is measured, then wavelength and incident angle dependent the most enhanced magnitude of e-field ($|\mathbf{E}|$) of the sample system are contour plotted as shown in Fig. 3. In addition, wavelength and incident angle with the maximum point of the $|\mathbf{E}|$ is denoted as the green dot. Figure 3(a) shows a contour plot of $|\mathbf{E}|$ depending on wavelength and incident angle in the array of Au NPs on PDMS substrate (Fig. 2(a)). As the light wavelength increases in the order of 500 nm, 600 nm, 700 nm, and 800 nm, the $|\mathbf{E}|$ is gradually bigger. On the contrary, the incident angle dependence is relatively little. The maximum $|\mathbf{E}|$

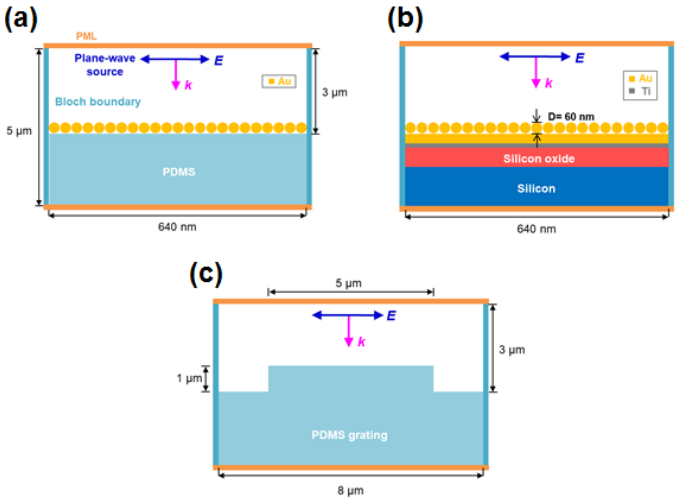

Fig. 2. (Color online) FDTD structures of the sample systems for the control experiments. (a) The array of Au NPs on PDMS substrate, (b) The array of Au NPs on Au film with Ti buffer layer on silicon dioxide deposited silicon substrate, and (c) PDMS line grating.

($|\mathbf{E}_{\mathrm{Max}}|$) is 9.7 V/m at the wavelength of 800 nm and incident angle of 0°. In case of the array of Au NPs on Au film-coated substrate, as similar as the array of Au NPs on PDMS substrate, the $|\mathbf{E}|$ becomes larger with increasing wavelength and changes relatively little as shown in Fig. 3(b). However, the $|\mathbf{E}_{\mathrm{Max}}|$ is 18.1 V/m, that is almost twice large than that in Fig. 3(a), at the wavelength of 800 nm and the incident angle of 0°. On the other hands, the wavelength and incident angle dependent $|\mathbf{E}|$ of the PDMS grating shows a plot with different tendency. As the incident angle increases in the order of 0°, 15°, 30°, and 45°, the $|\mathbf{E}|$ increases and decreases again at 60°. For wavelength dependence, it seems that the $|\mathbf{E}|$ oscillates as the wavelength increases as shown in Fig. 3(c). The $|\mathbf{E}_{\mathrm{Max}}|$ is 1.54 V/m at the wavelength of 600 nm and incident angle of 45°, which is smaller than the $|\mathbf{E}_{\mathrm{Max}}|$ obtained in the plasmonic sample system (Figs. 3(a) and 3(b)).

To characterize the wavelength and incident angle dependence on the $|\mathbf{E}|$ of the control sample systems, e-field profile at the $|\mathbf{E}_{\mathrm{Max}}|$ of the sample systems (points denoted by the green dots) are displayed as shown in Fig. 4. Figure 4(a) and 4(b) represent e-field profile near the array of Au NPs at the green dots denoting positions in Figs 3(a) and 3(b), respectively. As expected, the strongly enhanced e-field is observed in gaps between the Au NPs, which means that plasmonic excitation is a

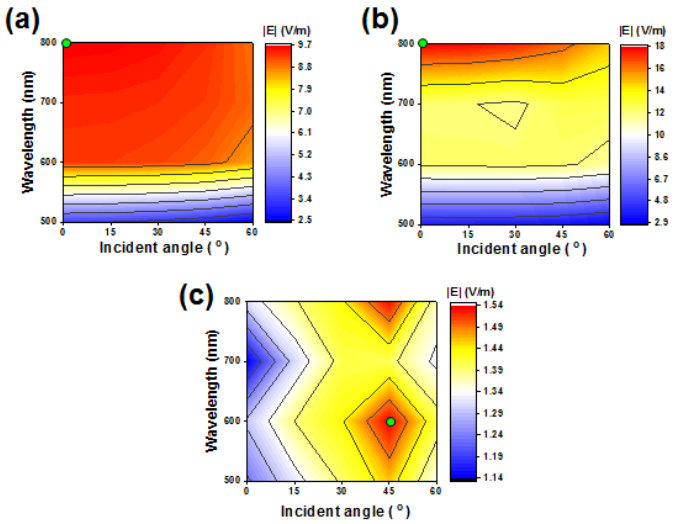

Fig. 3. (Color online) Contour plots of wavelength and incident angle of the light dependent $|\mathbf{E}|$ of the sample systems shown in Fig. 2. (a) The array of Au NPs on PDMS substrate, (b) the array of Au NPs on the Au film-coated substrate, and (c) PDMS line grating. The green dots denote the $|\mathbf{E}_{\mathrm{Max}}|$.

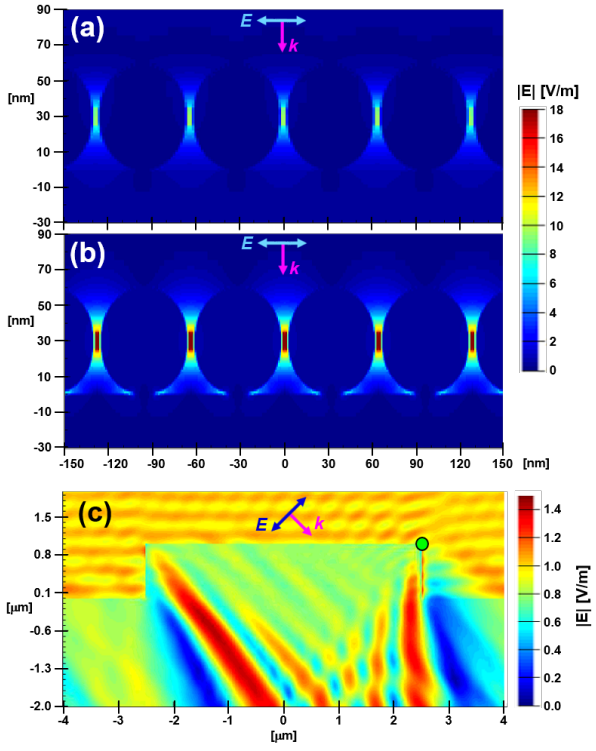

Fig. 4. (Color online) E-field profiles at wavelength and incident angle conditions for the $|\mathbf{E}_{\mathrm{Max}}|$ obtained in Fig. 3. (a) Array of Au NPs on PDMS substrate, (b) array of Au NPs on the Au film-coated substrate, and (c) PDMS line grating. The green dot denotes the position of the $|\mathbf{E}_{\mathrm{Max}}|$.

source of the e-field enhancement. As well as the $|\mathbf{E}|$ is much stronger in gaps of the Au NP array on Au film, e-filed enhancement is also shown between the Au NPs and the Au film. It would be regarded that the Au film underneath the Au NP array makes an effect to enhance e-field. Also, the increasing $|\mathbf{E}|$ with longer wavelength would be explained by general slit width and wavelength dependent diffraction; diffraction is more clearly generated in narrow slit width. In our system, the gap of the Au NP array is fixed as 4 nm and the wavelength varies. It can be considered that relatively longer wavelength of the light (800 nm) gets through the slit of smaller ratio (width to wavelength) than the shorter wavelength (500 nm); hence, it is assumed that strengthened diffraction would influence on the e-field enhancement. In case of e-field profile of the PDMS grating, the most enhanced e-field position is observed at the edge of the grating (the green dot in Fig. 4(c)). Figure 4(c) shows enhanced e-field inside of the PDSM grating; however, we exclude the e-field enhancement inside of the grating because Au NPs cannot be placed inside of the grating (no coupling between the grating and the plasmonic particles).

In order to investigate on influence of the grating effect on the plasmonic particles, the array of Au NPs on the PDMS grating (Fig. 5(a)) and the Au film-coated substrate (Fig. 5(b)) are designed. Figure 5(a) shows that array of Au NPs (60 nm diameter and 4 nm gap) is placed on the PDMS grating (5 μm width, 3 μm gap, and 1 μm height). On the other hand, the PDMS grating placing on the array of Au NPs on Au film-coated substrate is shown in Fig. 5(b). After measurements of FDTD simulations in all wavelengths and incident angles, contour plots of the $|\mathbf{E}|$ depending on wavelength and incident angle in the array of Au NPs on the PDMS grating (Fig. 5(a)) and sandwiched between the PDMS grating and the Au film-coated substrate (Fig. 5(b)) are displayed in Figs. 6(a) and 6(b), respectively. In Fig. 6(a), the $|\mathbf{E}_{\mathrm{Max}}|$ of 21.8 V/m is obtained at wavelength of 600 nm and incident angle of 45°, which is over twice larger than that in the array of Au NPs on PDMS substrate (Figs. 2(a) and 3(a)). It can be assumed that the PDSM grating makes an effect on the e-field enhancement, because the $|\mathbf{E}_{\mathrm{Max}}|$ appears at the same wavelength and incident angle with the PDMS grating case (Fig. 3(c)). On the other hands, the $|\mathbf{E}_{\mathrm{Max}}|$ of 38.7 V/m is obtained at the wavelength of 700 nm and incident angle of 45° in case

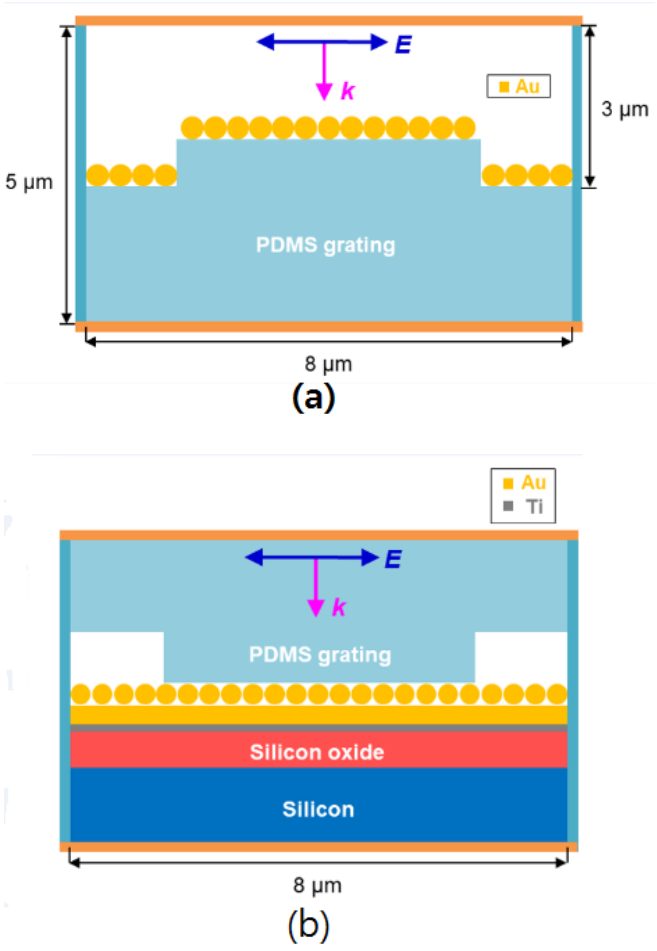

Fig. 5. (Color online) FDTD structures of the grating coupled plasmonic sample systems. (a) The array of Au NPs on PDMS grating and (b) PDMS contacting on the array of Au NPs on the Au film-coated substrate.

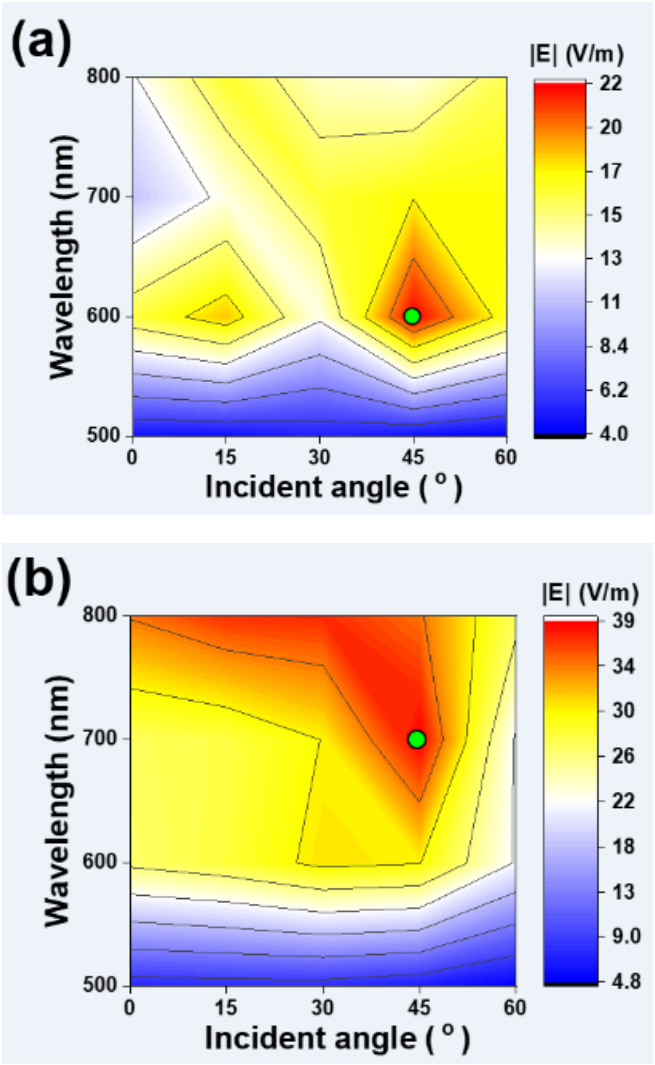

Fig. 6. (Color online) Contour plots of wavelength and incident angle of the light dependent $|\mathbf{E}|$ of the grating coupled plasmonic sample systems shown in Fig. 5. (a) The array of Au NPs on PDMS grating and (b) PDMS contacting on the array of Au NPs on the Au film-coated substrate. The green dots denote the $|\mathbf{E}_{\mathrm{Max}}|$.

of the array of Au NPs on the Au film-coated substrate (Fig. 6(b)). Figure 6(b) shows that the $|\mathbf{E}|$ increments with increasing wavelength as similar as Fig. 3(b) (the contour plot of $|\mathbf{E}|$ in the array of Au NPs on Au film substrate). But the $|\mathbf{E}_{\mathrm{Max}}|$ is shown at wavelength of 700 nm and incident angle of 45°, which seems to be influenced by the PDMS grating effect. In addition, the second $|\mathbf{E}_{\mathrm{Max}}|$ is 37.2 V/m at wavelength of 800 nm and incident angle of 30°, where it is near to the first $|\mathbf{E}_{\mathrm{Max}}|$ position. Tendency of wavelength and incident angle dependent the $|\mathbf{E}_{\mathrm{Max}}|$ of the PDMS grating contacting on the array of Au NPs on Au film-coated substrate (Fig. 6(b)) is distinguishable from that of the array of Au NPs on the PDMS grating (Fig. 6(a)), which would result from inletting light through the PDMS medium (not air) to reach the array of Au NPs.

The e-field profile at the condition and position for the $|\mathbf{E}_{\mathrm{Max}}|$ of the sample systems (the green dots in Fig. 6) are displayed in Fig. 7. Figure 7(a) shows e-field profile of the array of Au NPs on PDMS grating at the condition for the $|\mathbf{E}_{\mathrm{Max}}|$ (600 nm wavelength and 45° incident angle). The $|\mathbf{E}_{\mathrm{Max}}|$ is observed at the surface of the protruded grating structure (the red-dashed box in Fig. 7(a)). The e-field is most strongly enhanced (21.8 V/m) in gaps between the Au NPs. In case of the PDMS grating contacting on the array of Au NPs on Au film-coated substrate at the condition for the $|\mathbf{E}_{\mathrm{Max}}|$ (700 nm wavelength and 45° incident angle), the $|\mathbf{E}_{\mathrm{Max}}|$ is observed at

the Au NPs sandwiched between surfaces of the PDMS grating and the Au film-coated substrate as denoted by the red-dashed box in Fig. 7(b). The e-field is most strongly enhanced (38.7 V/m) in gaps between the Au NPs. Interestingly, e-field between the Au NPs and the Au film is also strongly enhanced, which is also observed in the array of Au NPs on Au film-coated substrate (Fig. 4(b)). Hence, it would be regarded that the Au film underneath the Au NP array makes an effect to enhance e-field in the PDMS grating contacting on the array of Au NPs on Au film substrate sample.

To clearly characterize e-field enhancement in the sample systems, a bar graph of the $|\mathbf{E}_{\mathrm{Max}}|$ in the sample systems is displayed as shown in Fig. 8. Comparing the $|\mathbf{E}_{\mathrm{Max}}|$ of the control sample systems, it turns out that e-field generated in plasmonic particles (the array of Au NPs) can be enhanced nearly twice (18.1 Vm^{-1}/9.7 Vm^{-1} =1.87) by placing on the Au film-coated substrate. Especially, by means of utilizing grating structure, e-field of the plasmonic particles can be enhanced over than twice; e-field enhancement is 2.25 (21.8 Vm^{-1}/9.7 Vm^{-1}) for the array of Au NPs on PDMS grating and that is 2.14 (38.7 Vm^{-1}/18.1 Vm^{-1}) for the PDMS grating contacting on array of Au NPs on Au film-coated substrate.

IV. Summary

By means of FDTD simulation analysis, e-field enhancement in the model systems of grating coupled plasmonic particles is characterized. The $|\mathbf{E}_{\mathrm{Max}}|$ is obtained in gaps between the Au NPs, and its dependence on the wavelength and incident angle of the light is influenced by the PDMS grating in the PDMS grating coupled Au NP array samples. In conclusion, it turns out that the $|\mathbf{E}_{\mathrm{Max}}|$ can be enhanced more than twice larger by utilizing the PDMS grating; which means that SERS signal of the plasmonic particles can be enlarged by electromagnetic enhancement with coupling with a dielectric grating. In addition, Au NP array on an Au film-coated substrate can be empirically obtained by lithographic approach combing with self-assembly of the nanoparticles [22–24]. Hence, this finding will be helpful to develop SERS applications, including an effective SERS template, in the future.

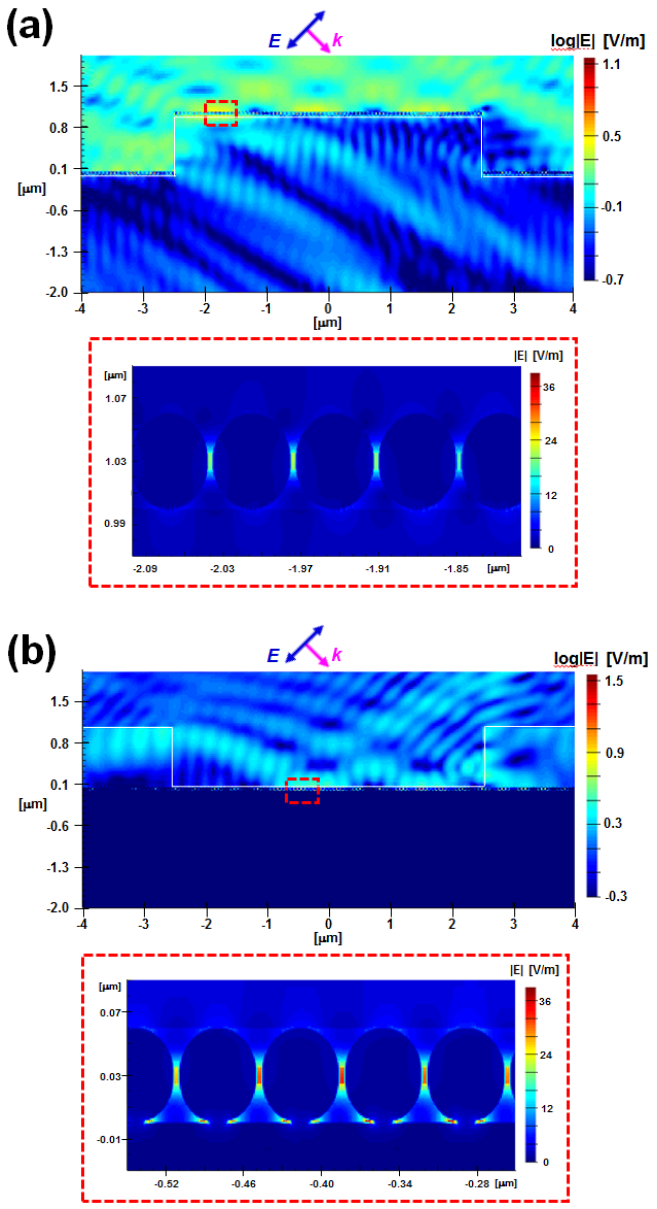

Fig. 7. (Color online) E-field profiles at wavelength and incident angle conditions for the $|\mathbf{E}_{\mathrm{Max}}|$ obtained in Fig. 6. (a) The array of Au NPs on PDMS grating and (b) PDMS contacting on the array of Au NPs on the Au film-coated substrate. The red dashed boxes denote regions of the $|\mathbf{E}_{\mathrm{Max}}|$, and the zoomed-in images are displayed in right.

ACKNOWLEDGEMENTS

This work was supported by a Research Grant of Pukyong National University(2017 year).

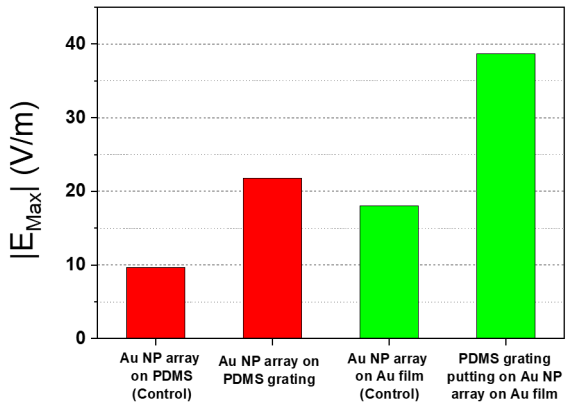

Fig. 8. (Color online) A bar graph of the $|\mathbf{E}_{\mathrm{Max}}|$ obtained in the control and grating effect coupled samples.

REFERENCES

[1] E. C. Le Ru, E. Blackie, M. Meyer and P. G. Etchegoin, J. Phys. Chem. C **111**, 13794, (2007).

[2] J. Reguera, J. Langer, D. Jiménez de Aberasturi and L. M. Liz-Marzán, Chem. Soc. Rev. **46**, 3866, (2017).

[3] M. A. Fikiet, S. R. Khandasammy, E. Mistek and Y. Ahmed *et al.*, Spectrochim. Acta A. **197**, 255, (2018).

[4] S. Schlücker, Angew. Chem. Int. Ed. **53**, 4756, (2014).

[5] J. Ryu, S. -H. Lee, Y. -H. Lee and Y. H. Chang *et al.*, J. Phys. Chem. C **123**, 5626, (2019).

[6] F. Hao, C. L. Nehl, J. H. Hafner and P. Nordlander, Nano Lett. **7**, 729, (2007).

[7] P. S. Kumar, I. Pastoriza-Santos, B. Rodríguez-González1 and F J. G. de Abajo *et al.*, Nanotechnology **19**, 015606, (2007).

[8] H. Yuan, C. G. Khoury, H. Hwang and C. M. Wilson *et al.*, Nanotechnology **23**, 075102, (2012).

[9] X. Tu, Z. Li, J. Lu and Y. Zhang *et al.*, RSC Adv. **8**, 2887, (2018).

[10] A. Campion and P. Kambhampati, 1. Chem. Soc. Rev. **27**, 241, (1998).

[11] P. L. Stiles, J. A. Dieringer, N. C. Shah and R. P. V. Duyne, 1. Annu. Rev. Anal. Chem. **1**, 601, (2008).

[12] P. A. Mosier-Boss, Nanomaterials **7**, 142, (2017).

[13] J. Deng, J. Dong and P. Cohen, Procedia Manuf. **26**, 580, (2018).

[14] P. Cheben, D. X. Xu, S. Janz and A. Densmore, Opt. Express **14**, 4695, (2006).

[15] P. J. Bock, P. Cheben, J. H. Schmid, J. Lapointe *et al.*, Opt. Express **18**, 16146, (2010).

[16] A. Llobera, R. Wilke and S. Büttgenbach, Lab Chip **4**, 24, (2004).

[17] P. B. Johnson and R. W. Christy, 1. Phys. Rev. **6**, 4370, (1972).

[18] J. H.Weaver, and H. P. R. Frederikse, "Optical properties of metals and semiconductors," in CRC Handbook of Chemistry and Physic 74th edition, David R. Lide (CRC Press, Inc., Florida, 1993-1994.), pp. 12-109.

[19] E. D. Palik, *Handbook of Optical Constants of Solids* (Academic press, 1985).

[20] M. H. Jang, J. K. Kim and H. Yoo, J. Nanosci. Nanotechnol. **12**, 4088 (2012).

[21] J. Lee, B. Hua, S. Park and M. Ha *et al.*, Nanoscale **6**, 616, (2014).

[22] M.-S. Yang, S. -J. Son, B. Park, B. K. Moon *et al.*, J. Appl. Phys. **114**, 234306, (2013).

[23] M.-S. Yang, S. -H. Lee, B. K. Moon, S. R. Yoo *et al.*, J. Appl. Phys. **120**, 085304, (2016).

[24] M.-S. Yang, C. Song, J. Choi, J. -S. Jo *et al.*, Nanoscale **11**, 2326, (2019).